Investigation of relayed nuclear Overhauser enhancement effect at –1.6 ppm in an ischemic stroke model

Lee Sze Foo[1], James R. Larkin[2], Brad A. Sutherland[3], Kevin J. Ray[2], Wun-She Yap[1], Choon-Hian Goh[1], Yan Chai Hum[1], Khin Wee Lai[4], George Harston[5], Yee Kai Tee[1]^

[1]Lee Kong Chian Faculty of Engineering and Science, Universiti Tunku Abdul Rahman, Kajang, Malaysia; [2]Department of Oncology, Cancer Research UK and Medical Research Council Oxford Institute for Radiation Oncology, University of Oxford, Oxford, UK; [3]Tasmanian School of Medicine, College of Health and Medicine, University of Tasmania, Hobart, Australia; [4]Faculty of Engineering, Department of Biomedical Engineering, University of Malaya, Kuala Lumpur, Malaysia; [5]Acute Stroke Service, Oxford University Hospitals National Health Service Foundation Trust, Oxford, UK

Contributions: (I) Conception and design: LS Foo, JR Larkin, BA Sutherland, YK Tee; (II) Administrative support: WS Yap, CH Goh; (III) Provision of study materials or patients: JR Larkin, BA Sutherland, KJ Ray; (IV) Collection and assembly of data: JR Larkin, BA Sutherland, KJ Ray, YC Hum; (V) Data analysis and interpretation: LS Foo, YC Hum, KW Lai, G Harston; (VI) Manuscript writing: All authors; (VII) Final approval of manuscript: All authors.

Correspondence to: Yee Kai Tee, DPhil. Lee Kong Chian Faculty of Engineering and Science, Universiti Tunku Abdul Rahman, Jalan Sungai Long, Bandar Sungai Long, Cheras 43000, Kajang, Selangor, Malaysia. Email: teeyeekai@gmail.com; teeyk@utar.edu.my.

Background: When an ischemic stroke happens, it triggers a complex signalling cascade that may eventually lead to neuronal cell death if no reperfusion. Recently, the relayed nuclear Overhauser enhancement effect at –1.6 ppm [NOE(–1.6 ppm)] has been postulated may allow for a more in-depth analysis of the ischemic injury. This study assessed the potential utility of NOE(–1.6 ppm) in an ischemic stroke model.

Methods: Diffusion-weighted imaging, perfusion-weighted imaging, and chemical exchange saturation transfer (CEST) magnetic resonance imaging (MRI) data were acquired from five rats that underwent scans at 9.4 T after middle cerebral artery occlusion.

Results: The apparent diffusion coefficient (ADC), cerebral blood flow (CBF), and apparent exchange-dependent relaxations (AREX) at 3.5 ppm and NOE(–1.6 ppm) were quantified. AREX(3.5 ppm) and NOE(–1.6 ppm) were found to be hypointense and exhibited different signal patterns within the ischemic tissue. The NOE(–1.6 ppm) deficit areas were equal to or larger than the ADC deficit areas, but smaller than the AREX(3.5 ppm) deficit areas. This suggested that NOE(–1.6 ppm) might further delineate the acidotic tissue estimated using AREX(3.5 ppm). Since NOE(–1.6 ppm) is closely related to membrane phospholipids, NOE(–1.6 ppm) potentially highlighted at-risk tissue affected by lipid peroxidation and membrane damage. Altogether, the ADC/NOE(–1.6 ppm)/AREX(3.5 ppm)/CBF mismatches revealed four zones of increasing sizes within the ischemic tissue, potentially reflecting different pathophysiological information.

Conclusions: Using CEST coupled with ADC and CBF, the ischemic tissue may thus potentially be separated into four zones to better understand the pathophysiology after stroke and improve ischemic tissue fate definition. Further verification of the potential utility of NOE(–1.6 ppm) may therefore lead to a more precise diagnosis.

Keywords: Ischemic stroke; chemical exchange saturation transfer (CEST); relayed nuclear Overhauser enhancement (NOE); amide proton transfer (APT); penumbra

^ ORCID: 0000-0002-0263-6358.

Introduction

During ischemic stroke, vascular occlusion triggers a complex signaling cascade that ultimately leads to neuronal cell death. This serial of multi-step pathophysiological events is known as the ischemic cascade (*Figure 1*). Briefly, the reduced blood flow causes anaerobic glycolysis and tissue acidosis, ionic pump failure and anoxic depolarization, causing increased glutamate release, and an elevation in intracellular calcium. This is then followed by mitochondrial collapse, cytotoxic edema, increased nitric oxide generation, and the production of free radicals which results in lipid peroxidation, leading to apoptosis or necrosis (1,2).

The purpose of acute stroke reperfusion treatment is to salvage as much viable tissue as possible prior to cell death; this tissue is known as the penumbra. However, the pathophysiology of stroke is complex, making the identification of the at-risk tissue a non-trivial task. The viability and size of the penumbra change dynamically depending on the regional blood flow, pathophysiological environment, and treatment (3). Thus, the ability to identify regions of tissue undergoing different stages or biochemical events within the ischemic cascade can reveal crucial information regarding the pathophysiology of the stroke tissue, and ultimately lead to a more precise diagnosis and therapeutic strategy.

Chemical exchange saturation transfer (CEST) is a magnetic resonance imaging (MRI) technique that works through the phenomenon by which saturation is transferred between solute and water molecules through chemical exchange (4,5). This contrast technique exploits the low-concentration solute molecules with exchangeable protons whose properties vary depending on the physiological conditions.

Thus far, the most widely studied form of CEST MRI is amide proton transfer (APT), originating from the backbone of proteins and peptides (6). APT is sensitive to intracellular pH changes (7) owing to the base-catalyzed amide proton exchange rate in the physiological range (8). As tissue acidosis occurs relatively early in the ischemic cascade (*Figure 1*), APT imaging is often proposed to be used as a biomarker for estimating the penumbra. Past studies have assessed the capability of APT imaging of supplementing conventional MRI in delineating the acidotic penumbra (9-16). While the results are promising, APT imaging provides mainly information on the tissue acidification of the ischemic injury.

Besides low-concentration metabolites, CEST MRI is also sensitive to nuclear Overhauser enhancement (NOE)-mediated effects that is related to spin interactions. Specifically, NOE is the transfer of nuclear spin polarization from one nuclear spin population to another via dipole-dipole cross-relaxation (17-19).

Previous studies have shown that for mobile proteins, the dominant mechanism for NOE effects observed upfield of water resonance is through intramolecular NOE from a non-exchangeable proton to an exchangeable proton, followed by chemical exchange between the exchangeable proton and bulk water (20-22), also known as relayed NOE. One of the most studied forms of relayed NOE effect is that resonating around −3.5 ppm (23). This relayed NOE effect is attributed to aliphatic protons and has been investigated particularly in neuro-oncology (24-27) as well as in ischemic stroke (28).

Recently, an increasing number of studies have investigated the relayed NOE effect resonating at −1.6 ppm [NOE(−1.6 ppm)] (19,29-31). In contrast to relayed NOE at −3.5 ppm, studies have shown the NOE(−1.6 ppm) signal to potentially arise from membrane choline (Cho) phospholipids, although the exact pathway of the observed effect is yet to be elucidated (32,33).

A crucial event in the ischemic cascade is the increased production of free radicals (*Figure 1*). These reactive oxygen species react irreversibly with cellular constituents including the double bonds of phospholipids, causing lipid peroxidation and membrane damage (2), which then leads to apoptosis or necrosis. Since lipid peroxidation occurs just before cell death, NOE(−1.6 ppm) related to membrane phospholipids may be sensitive to the consequent changes in the membrane, and can thus potentially act as a biomarker to identify tissue that is affected by lipid peroxidation and at immediate risk of cell death. This would provide vital information on a different stage of the ischemic cascade, allowing for a more in-depth analysis of the ischemic injury and thus precise diagnosis.
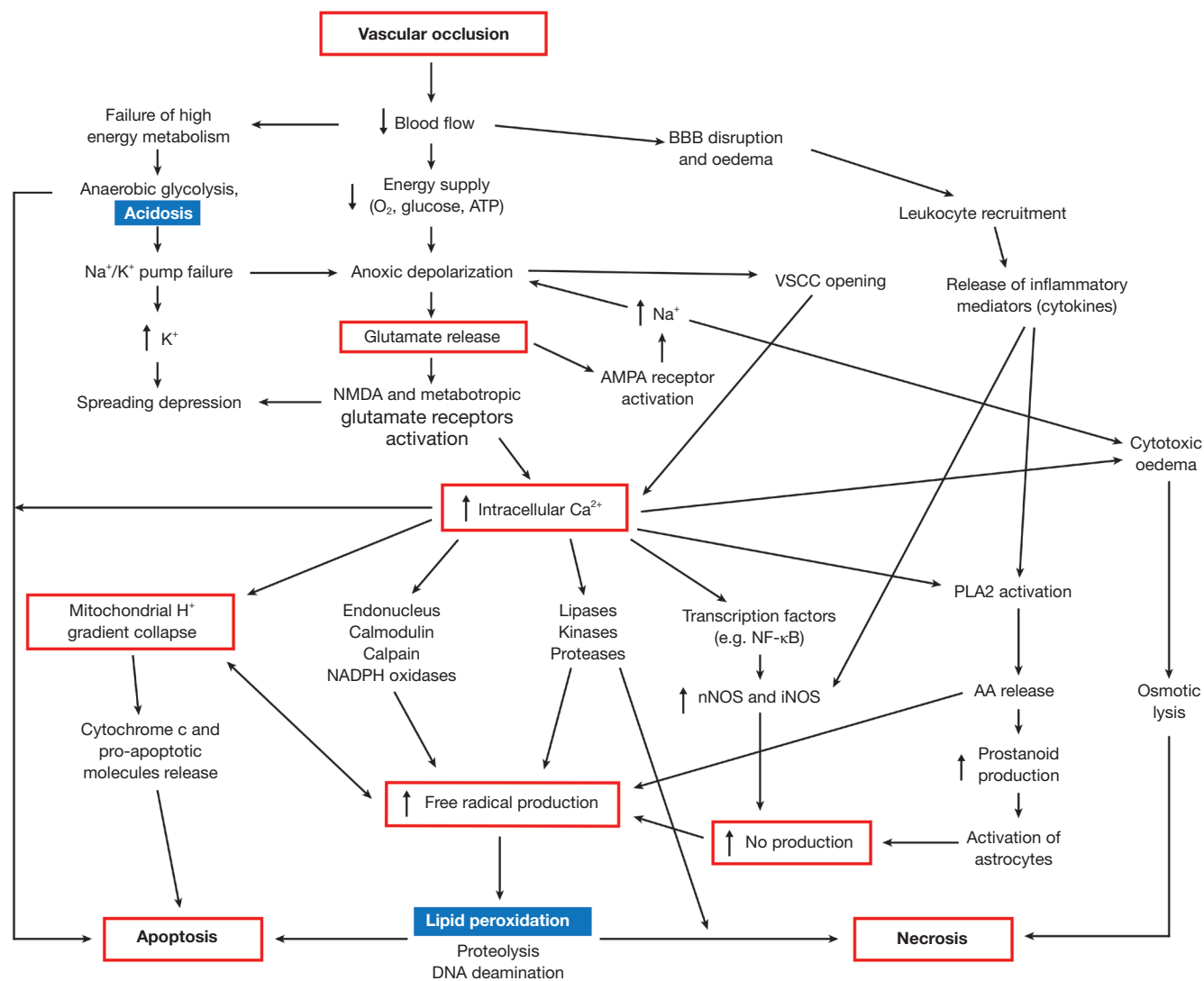
Figure 1 Ischemic cascade of biochemical events in the event of cerebral ischemia. The red boxes indicate the events of interest in CEST MRI; bold font represent important events. BBB, blood-brain barrier; ATP, adenosine triphosphate; VSCC, voltage sensitive calcium channel; AMPA, α-amino-3-hydroxy-5-methyl-4-isoxazolepropionic acid; NMDA, N-methyl-D-aspartate; NADPH, nicotinamide adenine dinucleotide phosphate; NF-κB, nuclear factor κB; nNOS, neuronal nitric oxide synthase; iNOS, inducible nitric oxide synthase; PLA2, phospholipase A2; AA, arachidonic acid; NO, nitric oxide. The figure was adapted from Sutherland *et al*. (1) with permission.

Previously, a 5-pool Lorentzian fitting was performed to quantify the NOE(–1.6 ppm) dip but the results were quite noisy and the NOE deficit area was only compared with diffusion deficit area (29). This study aimed to analyze NOE(–1.6 ppm) effect in an animal stroke model in a different way in order to determine the potential utility of NOE(–1.6 ppm) for ischemic stroke diagnosis to complement conventional MRIs such as diffusion and perfusion weighted imaging, as well as APT imaging. It is stipulated that the results may shed light on the implications of the observed effect and the new pathophysiological information revealed through NOE(–1.6 ppm) imaging.

Methods

Animal preparation

All animal experiments were approved by the Animal

Care and Ethical Review Committee of the University of Oxford and the Home Office (UK), in compliance with the University of Oxford Policy on the Use of Animals in Scientific Research and the Animals (Scientific Procedures) Act 1986 (UK). Reporting of animal experiments is in line with the ARRIVE guidelines. Intraluminal filament method, where a filament (Doccol, USA) was advanced up to the internal carotid artery was applied to induce middle cerebral artery occlusion (MCAO) (34) in six male Sprague Dawley rats around 8–10 weeks old and weighed in the low 200 g range, sourced from Envigo, UK. The filament remained in place throughout imaging. The CEST data of one of the rats was significantly noisy and was thus excluded; only data from the five remaining rats (referred to as Animals 1–5) were used for all subsequent analyses. The rats underwent MRI scans about 14 mins after MCAO.

MRI

All MRI experiments were carried out using a 9.4 T field strength scanner (Agilent, CA, USA). The images had spatial resolution of 0.5×0.5×1 mm^3 and 64×64 matrix size. T_1-weighted images were acquired using nine inversion times (TI) from 13.14–8,000 ms (repetition time/TR =10,000 ms, echo time/TE =27.16 ms); the scan took 3.35 mins. Diffusion-weighted images (DWI) were obtained at two b values –0 and 1,000 s/mm^2 in 31 seconds. A multi-phase pseudo-continuous arterial spin labeling (MP-PCASL) was applied at 8 radiofrequency (RF) phase offsets ranging from 0° to 315° with TE =28.68 ms and TR =4,000 ms. The label plane was placed around the neck, perpendicular to the carotid arteries, with the label duration of 1.4 s, comprising of a series of 600 μs long Hanning-shaped pulses with 600 μs separation and post-label delay of 0.55 s. Baseline signal intensity and reference images for coil sensitivity were acquired by omitting labelling pulses. The perfusion-weighted images (PWI) had an acquisition time of 1.48 min.

Multi-slice CEST images were acquired at the frequency offsets: 100, 72, 51, 37, 26, 19, 13.5, 9.7, 7, 5, 4.1, 3.9, 3.8, 3.7, 3.6, 3.5, 3.4, 3.3, 3.2, 3.1, 2.9, 2.7, 2.4, 2.1, 1.9, 1.8, 1.7, 1.6, 1.5, 1.2, 0.9, 0.6, 0.3, 0, –0.3, –0.6, –0.9, –1.2, –1.5, –1.7, –2, –2.3, –2.6, –2.9, –3.2, –3.5, –3.8 and –4.1. The unsaturated images were ±300 ppm. The saturation scheme used consisted of 50 primary and 5 secondary Gaussian pulses of 20 ms pulse duration and 50% duty cycle; three saturation flip angles (FAs) were acquired: 184°, 276°, and 366° (equivalent to average powers of 0.547, 0.820, and 1.088 μT respectively), and the secondary pulses were added to compensate for saturation loss during multi-slice acquisition. The total number of CEST slices was 10 with an in-plane 64×64 acquisition. The voxel size was 0.5×0.5×1 mm^3. Each CEST experiment had an acquisition time of 8.67 mins; TE =27.16 ms and TR =5 s. The average total acquisition time was about 120 mins because some animals took a longer time to be shimmed and some scans had to be repeated.

Data analysis

Apparent diffusion coefficient (ADC) maps were calculated as: $ADC = -\frac{1}{(b_2 - b_1)} \ln\left(\frac{S_{b_2}}{S_{b_1}}\right)$ where b_1=0 and b_2=1,000 s/mm^2. K-means clustering with $k = 2$ and K-means++ algorithm for center initialization seeding was used to automatically segment the ischemic lesions from the generated ADC maps (35-37) and a contralateral mask was manually drawn opposite to this. T_1 maps were obtained via mono-exponential fitting of the acquired signal intensities as a function of the inversion time (TI): $S = \left| a + c \times \exp\left(-\frac{TI}{T_1}\right) \right|$, where a and c are constants. Cerebral blood flow (CBF) maps were generated using a model-based fitting approach (38), where regions of similar phase offsets in the raw multiphase data were defined using supervoxel clustering which were then used to obtain high signal-to-noise ratio phase maps to produce calibrated CBF maps via a Bayesian multiphase fitting approach.

The collected CEST data were first normalized by the unsaturated image I_0, i.e., $Z(\Delta\omega) = \frac{I(\Delta\omega)}{I_0}$, where $I(\Delta\omega)$ is the CEST image at frequency offset $\Delta\omega$ and I_0 was the averaged signals at ±300 ppm. Then, the Z-spectra were smoothed using a moving average over a three-data point window to eliminate noise. Following this, the Z-spectra were corrected for B_0 inhomogeneity via voxel-wise single-Lorentzian curve fitting at frequency offsets assumed to only have direct water saturation (39)—within ±1.2 ppm and above/below ±6.0 ppm. The z-spectra were interpolated to the acquired frequency offset list above and –1.6 ppm after the B_0 inhomogeneity correction.

The APT signal was quantified using the apparent exchange-dependent relaxation (AREX) of the inhomogeneity-corrected CEST images as below (40):

$$MTR_{Rex}(\Delta\omega) = \frac{1}{Z(\Delta\omega)} - \frac{1}{Z_{ref}} \qquad [1]$$

$$AREX(\Delta\omega) = \frac{MTR_{Rex}(\Delta\omega)}{T_{1w}} \qquad [2]$$

where $\Delta\omega$ is the resonance frequency of the labile proton, in this case, $\Delta\omega = 3.5$ ppm, Z_{ref} is the reference signal at -3.5 ppm and T_{1W} is the water longitudinal relaxation time (41,42).

Additionally, the commonly used magnetization transfer ratio asymmetry at 3.5 ppm [MTR_{asym}(3.5 ppm)] was also calculated. The generated CEST images were smoothed using a 2×2 median filter.

NOE(-1.6 ppm) is not easy to be quantified because this transfer of magnetization effect is around the shoulder of the z-spectrum, may not be seen by direct observation of the z-spectrum and its effect is much smaller than the other commonly known effects such as APT and NOE(-3.5 ppm) (43,44). Although changes of the NOE(-1.6 ppm) had been reported by several studies (19,29-31), the quantified results were very noisy and huge signal variation was observed.

In this study, the NOE(-1.6 ppm) was quantified using a different approach, where the inverse of collected signal at -1.6 ppm, $Z(-1.6$ ppm) was first subtracted from a reference using the signal at 19 ppm, $Z(19$ ppm) normalized by the signal at 13.5 ppm, $Z(13.5$ ppm), i.e., $\frac{Z(19\,ppm)}{Z(13.5\,ppm)}$ and then divided by the water longitudinal relaxation time:

$$NOE\left(-1.6\,ppm\right) = \frac{\frac{1}{Z\left(-1.6\,ppm\right)} - \frac{Z\left(19\,ppm\right)}{Z\left(13.5\,ppm\right)}}{T_{1w}} \quad [3]$$

The reference signal, $\frac{Z(19\,ppm)}{Z(13.5\,ppm)}$ should be free from potential contaminations such as magnetization transfer (MT) and other CEST/rNOE exchange (45); the opposite offset (1.6 ppm) was not used as the reference as it may have contaminations from nearby CEST effects such as amine around 2 ppm which has been shown to alter significantly during ischemia due to slower amine proton exchange rate in an acidic environment (13,46); the quantified NOE signal is normalized by the water relaxation time because it is widely known that this will change significantly after stroke (35-37).

Relative NOE(-1.6 ppm) was calculated as: $ReNOE\left(-1.6\,ppm\right) = \frac{NOE\left(-1.6\,ppm\right)}{\left|mean\left(NOE_{normal}\left(-1.6\,ppm\right)\right)\right|}$, where $NOE_{normal}(-1.6$ ppm) is the quantified NOE signal in the contralateral normal appearing mask manually drawn opposite to the ischemic region. A two-tailed paired t-test was used to test for significant differences between the ReNOE(-1.6 ppm) within the ADC deficit and contralateral areas at 5% significance level.

To determine the optimal saturation power for maximum contrast between the ischemic and non-ischemic tissues, the contrast-to-noise ratio (CNR) of the NOE(-1.6 ppm) maps was evaluated as:

$$CNR = \frac{contrast}{Cov} \quad [4]$$

where contrast is:

$$contrast = \left| \frac{mean\left(NOE_{normal}\left(-1.6\,ppm\right)\right) - mean\left(NOE_{ischemic}\left(-1.6\,ppm\right)\right)}{mean\left(NOE_{normal}\left(-1.6\,ppm\right)\right) + mean\left(NOE_{ischemic}\left(-1.6\,ppm\right)\right)} \right| \quad [5]$$

and CoV is the coefficient of variation:

$$CoV = \frac{STD\left(NOE_{normal}\left(-1.6\,ppm\right)\right)}{\left|mean\left(NOE_{normal}\left(-1.6\,ppm\right)\right)\right|} \quad [6]$$

STD is the standard deviation.

All the generated CEST images were smoothed using a 2×2 median filter (43,44). To compare spatial heterogeneity patterns of the ADC, AREX(3.5 ppm), and NOE(-1.6 ppm) maps within the ischemic area, the two-dimensional gradients i.e., the directional changes of the voxels within the ADC deficit area were calculated:

$$\nabla F = \frac{\partial F}{\partial x}\hat{i} + \frac{\partial F}{\partial y}\hat{j} \quad [7]$$

where $F(x,y)$ is the image, i.e., the ADC, AREX(3.5 ppm), or NOE(-1.6 ppm) maps.

Lastly, the deficit areas of the AREX(3.5 ppm), NOE(-1.6 ppm), and CBF maps were also automatically segmented using K-means clustering, with some manual corrections verified by an experienced clinician. The binary masks of the segmented ADC, CBF, AREX(3.5 ppm), and NOE(-1.6 ppm) areas were overlaid to produce the mismatch maps of the deficit areas. All the data processing and analyses were performed using custom written functions in Matlabs on the biggest ADC deficit slice of each animal.

Results

Figure 2 shows the ADC and T_1 maps, as well as the 184º, 276º, 366º FA Z-spectra and NOE(-1.6 ppm) images of a representative animal (Animal 1). ADC was decreased in the ischemic area, while T_1 was hyperintense, consistent with previous findings (36). The segmented ADC deficit area (red) and the corresponding contralateral mask (blue) are overlaid on the MR images.

The CEST Z-spectra decreased in magnitude while the CEST dips broadened with increasing FA, as a result of the increased saturation power. A dip was observed around -1.6 ppm across all FAs. Upon generating the NOE(-1.6 ppm) maps, it was observed that the ischemic areas were hypointense, in line with a previous study (29), and coincided well with the ADC deficit area.
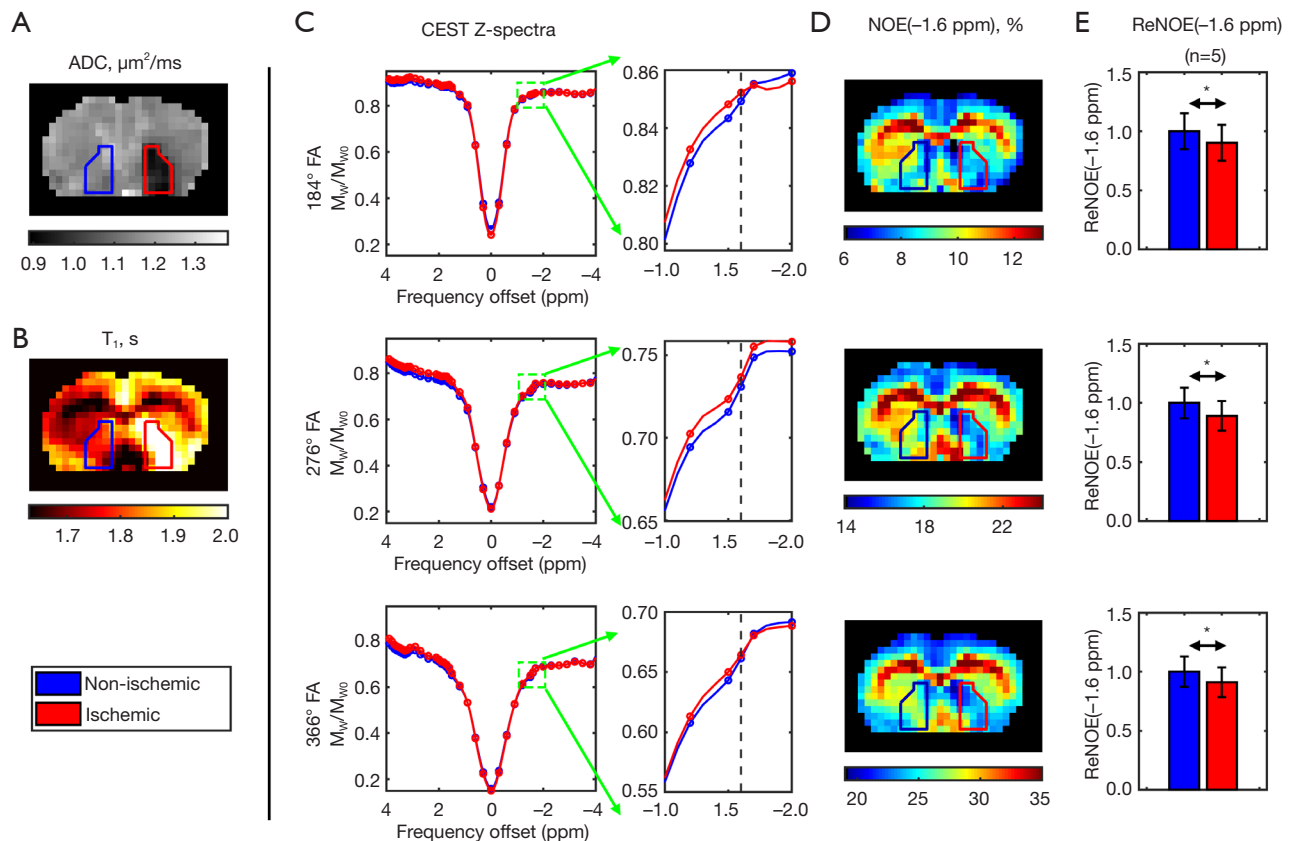
Figure 2 Representative results of the different magnetic resonance imaging data collected in this study. (A) ADC (µm²/ms), (B) T1 (s), (C) CEST Z-spectra, and (D) NOE(–1.6 ppm) at 184º, 276º, 366º saturation flip angles of a representative animal (Animal 1), along with (E) the bar chart of ReNOE(–1.6 ppm) of all animals (n=5). The ADC deficit (red) and contralateral (blue) areas are overlaid on the MR images. *, P<0.05. ADC, apparent diffusion coefficient; FA, flip angle; CEST, chemical exchange saturation transfer; NOE, nuclear Overhauser enhancement; ReNOE, relative nuclear Overhauser enhancement; MR, magnetic resonance.

The ReNOE(–1.6 ppm) of all five animals were found to have significant differences between the ischemic and non-ischemic tissues across all FAs.

The average NOE(–1.6 ppm) of all five animals increased from 184º to 366º FA in both ischemic and non-ischemic tissues (*Figure 3A*). The CNR of NOE(–1.6 ppm) between the two tissues was found to peak at 276º FA, with 184º FA producing the lowest CNR, followed by 366º, as shown in *Figure 3B*. Likewise, the CNR of AREX(3.5 ppm) and AREX(2 ppm) were also maximized at 276º FA (Figure S1). Since this FA produced the highest CNR in both NOE(–1.6 ppm) and AREX(3.5 ppm), the CEST/AREX/NOE maps at 276º FA were used for all subsequent analyses. The most commonly used metric, MTR_{asym}(3.5 ppm) was reported in Figure S2 to facilitate the comparison of results with the literature and future

studies.

Figure 4 shows the ADC, AREX(3.5 ppm), and NOE(–1.6 ppm) maps at 276º FA of three representative animals (Animal 1–3), overlaid with the spatial gradients within the ADC deficit areas, shown as arrows. The ADC within the deficit area was comparably more homogenous than the 3.5 ppm AREX map and –1.6 ppm NOE map. Comparing between the two maps, although both AREX(3.5 ppm) and NOE(–1.6 ppm) were hypointense within the ADC deficit area, the two maps exhibited different spatial signal variations within the deficit area, evidenced by the different gradient directions in the AREX(3.5 ppm) and NOE(–1.6 ppm) plots.

The deficit areas of the ADC, CBF, AREX(3.5 ppm), and NOE(–1.6 ppm) maps were further segmented in *Figure 5*. Both AREX(3.5 ppm) and NOE(–1.6 ppm)
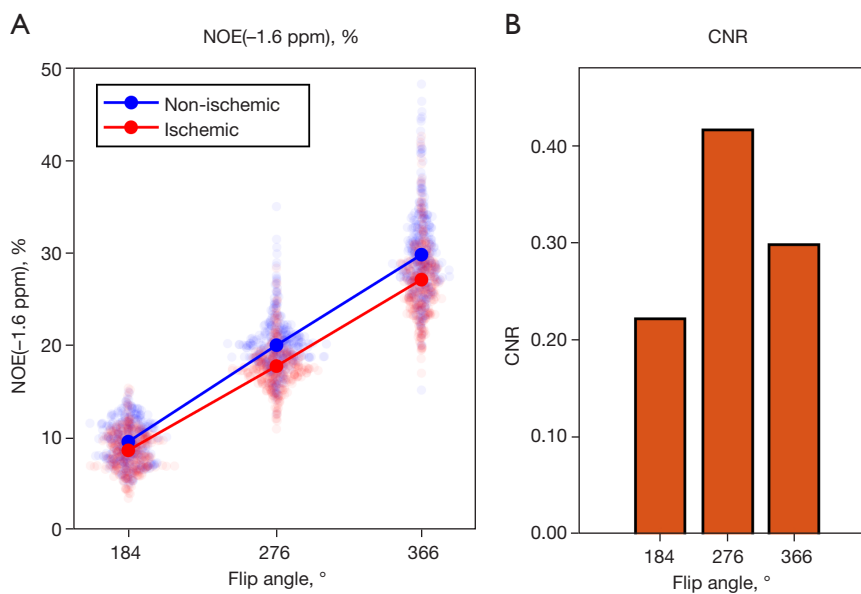
Figure 3 The NOE(–1.6 ppm) signal in the ischemic and non-ischemic tissues. (A) The average NOE(–1.6 ppm) of ischemic (red) and non-ischemic (blue) tissues are shown as line plots; the individual NOE(–1.6 ppm) values are visualized as SinaPlots (47). (B) CNR of the NOE(–1.6 ppm) between the two tissues. The flip angles: 184°, 276°, and 366° are equivalent to average powers of 0.547, 0.820, and 1.088 µT respectively. NOE, nuclear Overhauser enhancement; CNR, contrast-to-noise ratio.
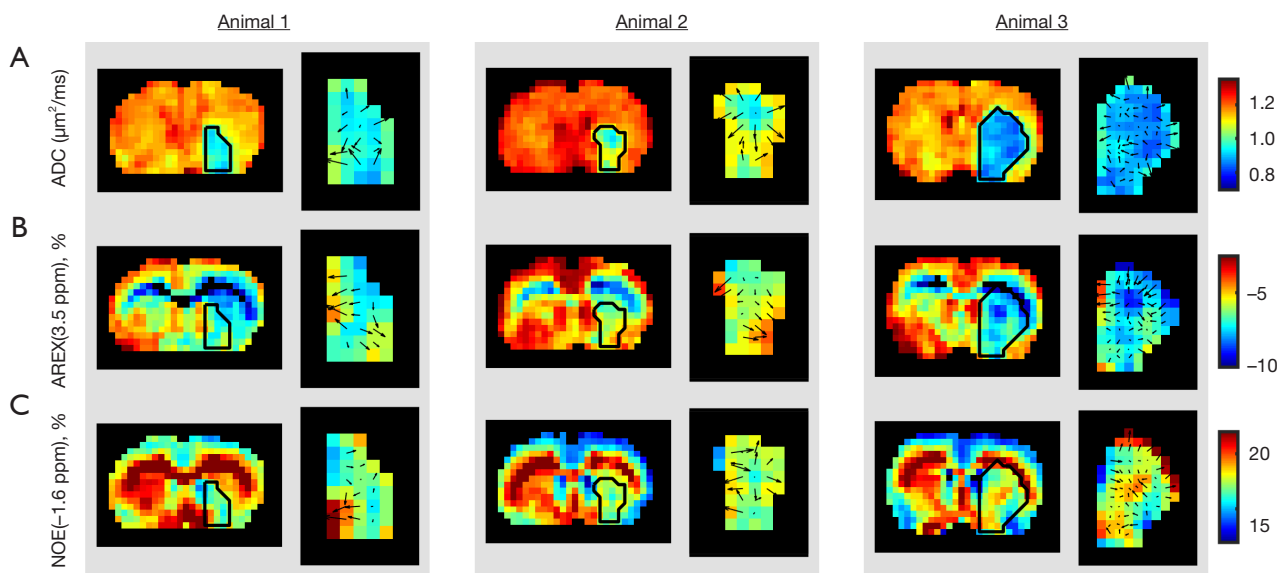

Figure 4 The quantified results of representative animals. The spatial gradients (arrows) of the (A) ADC, (B) AREX(3.5 ppm), and (C) NOE(–1.6 ppm) maps at 276° FA within the ADC deficit area of Animals 1–3. ADC, apparent diffusion coefficient; AREX, apparent exchange-dependent relaxation; NOE, nuclear Overhauser enhancement; FA, flip angle.
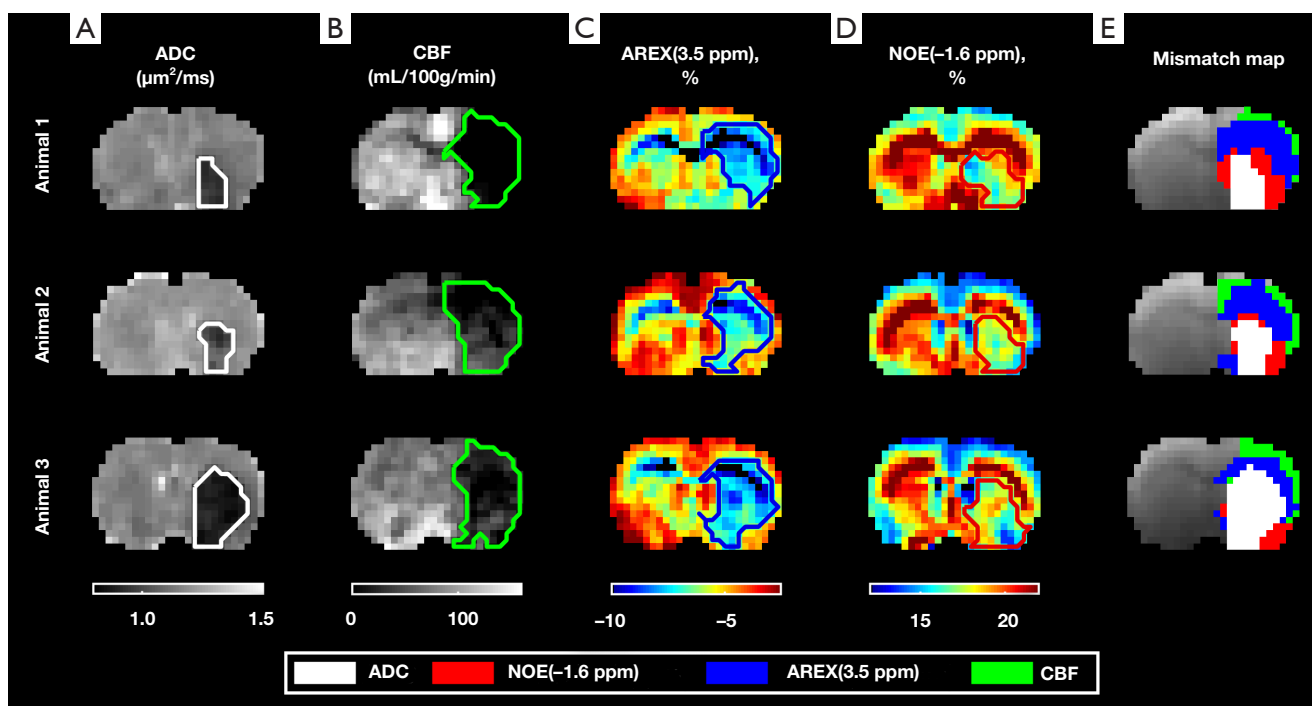
7886

Foo et al. Relayed NOE at –1.6 ppm in an ischemic stroke model

Figure 5 The ischemic masks in different magnetic resonance imaging results and mismatch maps of representative animals. The (A) ADC (white), (B) CBF (green), (C) AREX(3.5 ppm) (blue), and (D) NOE(–1.6 ppm) (red) deficit areas of Animals 1–3, and (E) the mismatch maps with display priority of white > red > blue > green. ADC, apparent diffusion coefficient; CBF, cerebral blood flow; AREX, apparent exchange-dependent relaxation; NOE, nuclear Overhauser enhancement.

produced deficit areas that coincided well with the ADC deficit areas. The AREX(3.5 ppm) deficit areas were intermediate in size between the ADC and CBF deficit areas. Conversely, the NOE(–1.6 ppm) deficit areas were found to be equal or larger than the ADC deficit areas, but smaller than the AREX(3.5 ppm) deficit areas. Altogether, the mismatch maps of the MRI deficit areas produced four regions of increasing sizes: ADC deficit (white) < NOE(–1.6 ppm) (red) < AREX(3.5 ppm) (blue) < CBF (green).

Discussion

This study analyzed NOE(–1.6 ppm) effect in animal stroke models in order to assess its potential utility in an ischemic stroke model. Several studies have sought to find possible origins of the relayed NOE effect resonating at –1.6 ppm. Zhang *et al.* first showed egg phosphatidylcholine (PtdCho) with cholesterol to exhibit the same NOE(–1.6 ppm) resonance observed in that of rat brain, suggesting the Cho phospholipids in cell membranes to be

related to the observed relayed NOE effect (31). Zu *et al.* also later verified the NOE(–1.6 ppm) signal to be sensitive to Cho phospholipids and the presence of cholesterol was also shown to be crucial in inducing the relayed NOE effect. *In vivo*, the signal possibly stems from the head groups of PtdCho and sphingomyelin (SM) as they are the major phospholipid components of eukaryotic cells (32).

Although Cho phospholipids are largely agreed to be related to NOE(–1.6 ppm), the exact pathway or mechanism of inducing the relayed NOE signal is still not well understood. The study by Zu *et al.* initially suggested the relayed NOE signal to be the dependent on the membrane fluidity and composition (32). However, a more recent publication by Chang *et al.* showed that the key to inducing the relayed NOE signal is not the lipid bilayer dynamics, but the hydroxyl group of cholesterol (33). Still, this has only been verified at the molecular level and thus further investigations are still needed to determine the pathway of the relayed NOE signal *in vivo*. Nevertheless, the studies largely agree that NOE(–1.6 ppm) effect potentially arises from membrane Cho phospholipids (31-33).

PtdCho is a major component of the phospholipid membrane of cells and has been shown to be broken down in response to cerebral ischemia (48). This loss is also associated with a breakdown of other phospholipids including SM (49) as well as activation of phospholipases (50). This results in free fatty acid formation and activation of enzymes such as cyclooxygenases and lipoxygenases that can lead to reactive oxygen species formation. The presence of free radicals can cause substantial lipid peroxidation and loss of cell integrity. This is a prominent part of the ischemic cascade, as strategies to restore phospholipid (PtdCho and SM) levels such as the use of CDP-choline can prevent lipid peroxidation, cell loss and could be used as a potential therapeutic treatment for stroke patients (49,51,52). Thus, the ability to identify regions of tissue affected by lipid peroxidation could contribute towards an improved therapeutic strategy.

From the results, it was found that NOE(–1.6 ppm) exhibited different signal variations within the ADC deficit area compared to AREX(3.5 ppm) (*Figure 4*), suggesting that the APT and NOE(–1.6 ppm) were sensitive to different changes within the ischemic tissue and thus relay information on separate stages or events in the ischemic cascade. Most notably, while the AREX(3.5 ppm) deficit areas were intermediate in size between the ADC and CBF deficit areas, the NOE(–1.6 ppm) deficit areas were observed to be smaller than the AREX(3.5 ppm) deficit areas but larger than or equal in size to the ADC deficit areas (*Figure 5*). This suggested that the NOE(–1.6 ppm) maps further delineated the ADC/AREX(3.5 ppm) mismatch into zones of normal and decreased NOE(–1.6 ppm) effect. Since NOE(–1.6 ppm) effect is related to the membrane phospholipids, it is possible that the NOE(–1.6 ppm) is sensitive to the lipid peroxidation of the membranes, and its deficit area highlighted the tissue with potential membrane damage and tissue close to cell death (*Figure 1*).

Previous studies on APT imaging of ischemic stroke focused on its use to separate the DWI/PWI mismatch into zones of acidotic penumbra and benign oligemia (53-55), as was also observed in the present study. The findings of the present study thus builds on this, demonstrating that the use of NOE(–1.6 ppm) may further delineate the ADC/AREX(3.5 ppm) mismatch into zones of tissue affected by lipid peroxidation and membrane damage, and those that were not. When analyzed together, the DWI/NOE(–1.6 ppm)/APT/PWI mismatch map revealed four regions within the ischemic tissue, possibly: the ischemic infarct, at-risk tissue undergoing lipid peroxidation and membrane damage, acidotic at-risk tissue, and the benign oligemia. Therefore, the use of NOE(–1.6 ppm) CEST MRI has the potential to allow for a better understanding of stroke pathophysiology and improve tissue fate definition, thus achieving a more precise diagnosis. Nevertheless, it is not possible to rule out that there may be a potential change of the lesion size, MRI and tissue parameters (e.g., relaxation rates, pH, etc.) over the course of MRI acquisitions that could affect the observed mismatch maps. In any case, histopathology and further studies are still needed to elucidate the origins or observed changes of NOE(–1.6 ppm).

It is worth noting that NOE(–1.6 ppm) effect may not be visible using clinical scanners with low field strengths of 3 T and below as the induced effect is very small and close to the water center frequency. Nevertheless, recent years have seen the rapid methodological and hardware developments of ultrahigh magnetic field clinical MRI particularly at 7 T, and an increasing usage of 7 T MR scanners for human imaging (56). The implementation of high field strength scanners would thus enable the investigation of NOE(–1.6 ppm) at the clinical level (23).

In addition to the aforementioned elusive signal inducing pathway, the changes in NOE(–1.6 ppm) proton pool in ischemic tissue that result in the changes in the observed effect is also currently not well understood. In order to speculate possible explanations for this, numerical simulation of a six-pool CEST model using average experimental water relaxation times and parameters taken from literature (57-62) was performed (see Appendix 1). The concentration of the NOE(–1.6 ppm) pool of ischemic tissue was kept constant while the exchange rate was varied with a range of values (decrease by 30–50% of the normal value) to match the observed trends in the experimental data as seen in *Figure 3*. Although the concentration is also expected to change in ischemic tissue, it is difficult to isolate the concentration effects from the exchange rate as the two have the same effect on the observed signal. In order to estimate the effective changes in the proton pool after stroke, changes in the proton concentration were assumed to be negligible, as stipulated by Zhou *et al.* in the case of early time point stroke (8). The simulation results suggested that the observed decrease in NOE(–1.6 ppm) was likely due to a reduction in the NOE(–1.6 ppm) exchange rate by 44% of the normal value if the concentration did not change (Figure S3). Still, further studies involving proteomics are recommended to shed light on the percentage of concentration change and determine the isolated changes in all the pool concentration and exchange rate after stroke (63).

In this study, K-means clustering was used to automatically segment the deficit areas of the MR images as it is difficult to differentiate between the gray and white matter of the rat brains manually due to the small volume and low resolution of the images. Although this approach differs from the clinical gold standard of having experienced radiologists drawing the regions-of-interests manually, automatic segmentation allows for more reproducible results. However, due to the small size of the rat brains, the automatic segmentation of the deficit areas may have included the ventricles. Additionally, the small sample size was also one of the limitations of the study.

Multi-pool Lorentzian fits are another popular method to quantify the various CEST and relayed NOE effects, but it is not easy to have a reliable fit at −1.6 ppm due to the magnitude of this effect and its small frequency separation with the water. For more reliable signal quantification at −1.6 ppm, it is suggested to first smooth the acquired Z-spectra with a moving average to minimize noise and then only quantify it using Eq. [3] with reference signal not affected by any known exchange effect and normalized by a nearby saturated signal, e.g., $Z(19 \text{ ppm})/Z(13.5 \text{ ppm})$. It is believed that the quantified NOE(−1.6 ppm) in this study is more 'clean' because longitudinal relaxation time which is widely known to change after stroke, has been minimized by dividing it with T_1 and the reference signal [$Z(19 \text{ ppm})/Z(13.5 \text{ ppm})$] is minimally effected by MT and other factors; the reference signal can be a ratio of any two neighboring offsets that are free from any known CEST or NOE. Nevertheless, it is possible that direct saturation as well as relayed NOE at −3.5 ppm and potentially some minor effect from MT at −1.6 ppm could still affect the quantified NOE(−1.6 ppm). In order to ensure optimal and reliable NOE(−1.6 ppm) could be obtained, the experiments were repeated with three different saturation powers. It was found that all the experiments showed consistent NOE(−1.6 ppm) effect after stroke using the proposed definition. This is the first study to show CEST imaging coupled with DWI and PWI may potentially separate the ischemic tissue into four zones to better understand the pathophysiology or the ischemic cascade after stroke. More investigations are needed to improve the specificity of the quantified relayed NOE at −1.6 ppm to support the observations, e.g., the most optimal way to quantify this small NOE signal, and to confirm that CEST can be used to detect the biochemical events of the ischemic cascade. In addition, the saturation time was not optimized in this study due to the time constraint in the induced stroke experiments.

Conclusions

CEST imaging of NOE(−1.6 ppm) that is related to membrane phospholipids shows potential in identifying ischemic tissue that is affected by lipid peroxidation and membrane damage, separate from the acidotic tissue estimated using APT. When the NOE(−1.6 ppm) deficit area is analyzed together with the DWI, APT and PWI deficit areas, the ischemic tissue could potentially be defined using information from four different sources. This can reveal important information regarding the complex pathophysiology of the stroke tissue and contribute to a more precise acute stroke diagnosis. Nevertheless, further studies are needed to elucidate the origins and observed changes of NOE(−1.6 ppm).

Acknowledgments

Footnote

Conflicts of Interest: All authors have completed the ICMJE uniform disclosure form (available at https://qims.amegroups.com/article/view/10.21037/qims-23-510/coif). YKT received support/funding from Ministry of Higher Education Malaysia under the Fundamental Research Grant Scheme (No. FRGS/1/2021/ICT02/UTAR/02/2), National Cancer Council Malaysia Cancer Research Award 2018 (No. 4363/T01), UTAR Research Fund (No. IPSR/RMC/UTARRF/2020-C1/T02), and a Quadro P6000 GPU from NVIDIA Corporation. GH reports that he is a part-time employee of and has stock options with Brainomix Ltd. JRL is an inventor of a patent related to ASL methodology and reports that this study was funded in part by Cancer

References

1. Sutherland BA, Minnerup J, Balami JS, Arba F, Buchan AM, Kleinschnitz C. Neuroprotection for ischaemic stroke: translation from the bench to the bedside. Int J Stroke 2012;7:407-18.

2. Durukan A, Tatlisumak T. Acute ischemic stroke: overview of major experimental rodent models, pathophysiology, and therapy of focal cerebral ischemia. Pharmacol Biochem Behav 2007;87:179-97.

3. Liu S, Levine SR, Winn HR. Targeting ischemic penumbra: part I - from pathophysiology to therapeutic strategy. J Exp Stroke Transl Med 2010;3:47-55.

4. Ward KM, Balaban RS. Determination of pH using water protons and chemical exchange dependent saturation transfer (CEST). Magn Reson Med 2000;44:799-802.

5. Ward KM, Aletras AH, Balaban RS. A new class of contrast agents for MRI based on proton chemical exchange dependent saturation transfer (CEST). J Magn Reson 2000;143:79-87.

6. Zhou J, Heo HY, Knutsson L, van Zijl PCM, Jiang S. APT-weighted MRI: Techniques, current neuro applications, and challenging issues. J Magn Reson Imaging 2019;50:347-64.

7. Tee YK, Harston GW, Blockley N, Okell TW, Levman J, Sheerin F, Cellerini M, Jezzard P, Kennedy J, Payne SJ, Chappell MA. Comparing different analysis methods for quantifying the MRI amide proton transfer (APT) effect in hyperacute stroke patients. NMR Biomed 2014;27:1019-29.

8. Zhou J, Payen JF, Wilson DA, Traystman RJ, van Zijl PC. Using the amide proton signals of intracellular proteins and peptides to detect pH effects in MRI. Nat Med 2003;9:1085-90.

9. Harston GW, Tee YK, Blockley N, Okell TW, Thandeswaran S, Shaya G, Sheerin F, Cellerini M, Payne S, Jezzard P, Chappell M, Kennedy J. Identifying the ischaemic penumbra using pH-weighted magnetic resonance imaging. Brain 2015;138:36-42.

10. Heo HY, Zhang Y, Burton TM, Jiang S, Zhao Y, van Zijl PCM, Leigh R, Zhou J. Improving the detection sensitivity of pH-weighted amide proton transfer MRI in acute stroke patients using extrapolated semisolid magnetization transfer reference signals. Magn Reson Med 2017;78:871-80.

11. Foo LS, Harston G, Mehndiratta A, Yap WS, Hum YC, Lai KW, Mohamed Mukari SA, Mohd Zaki F, Tee YK. Clinical translation of amide proton transfer (APT) MRI for ischemic stroke: a systematic review (2003-2020). Quant Imaging Med Surg 2021;11:3797-811.

12. Wu Y, Li H, Pei C, Sun PZ, Yin J. Discrimination between progressive penumbra and benign oligemia of the diffusion-perfusion mismatch region by amide proton transfer-weighted imaging. Magn Reson Imaging 2023;99:123-9.

13. Wu Y, Sun PZ. Demonstration of pH imaging in acute stroke with endogenous ratiometric chemical exchange saturation transfer magnetic resonance imaging at 2 ppm. NMR Biomed 2023;36:e4850.

14. Sun PZ. Quasi-steady-state amide proton transfer (QUASS APT) MRI enhances pH-weighted imaging of acute stroke. Magn Reson Med 2022;88:2633-44.

15. Larkin JR, Foo LS, Sutherland BA, Khrapitchev A, Tee YK. Magnetic Resonance pH Imaging in Stroke - Combining the Old With the New. Front Physiol 2021;12:793741.

16. Heo HY, Tee YK, Harston G, Leigh R, Chappell MA. Amide proton transfer imaging in stroke. NMR Biomed

2023;36:e4734.

17. Anderson WA, Freeman R. Influence of a second radiofrequency field on high-resolution nuclear magnetic resonance spectra. J Chem Phys 1962;37:85-103.

18. Solomon I. Relaxation processes in a system of two spins. Physical Review 1955;99:559-65.

19. Zu Z. Ratiometric NOE(-1.6) contrast in brain tumors. NMR Biomed 2018;31:e4017.

20. van Zijl PC, Zhou J, Mori N, Payen JF, Wilson D, Mori S. Mechanism of magnetization transfer during on-resonance water saturation. A new approach to detect mobile proteins, peptides, and lipids. Magn Reson Med 2003;49:440-9.

21. van Zijl PCM, Lam WW, Xu J, Knutsson L, Stanisz GJ. Magnetization Transfer Contrast and Chemical Exchange Saturation Transfer MRI. Features and analysis of the field-dependent saturation spectrum. Neuroimage 2018;168:222-41.

22. Jin T, Kim SG. Role of chemical exchange on the relayed nuclear Overhauser enhancement signal in saturation transfer MRI. Magn Reson Med 2022;87:365-76.

23. Jones CK, Huang A, Xu J, Edden RA, Schär M, Hua J, Oskolkov N, Zacà D, Zhou J, McMahon MT, Pillai JJ, van Zijl PC. Nuclear Overhauser enhancement (NOE) imaging in the human brain at 7T. Neuroimage 2013;77:114-24.

24. Heo HY, Jones CK, Hua J, Yadav N, Agarwal S, Zhou J, van Zijl PC, Pillai JJ. Whole-brain amide proton transfer (APT) and nuclear overhauser enhancement (NOE) imaging in glioma patients using low-power steady-state pulsed chemical exchange saturation transfer (CEST) imaging at 7T. J Magn Reson Imaging 2016;44:41-50.

25. Zaiss M, Windschuh J, Paech D, Meissner JE, Burth S, Schmitt B, Kickingereder P, Wiestler B, Wick W, Bendszus M, Schlemmer HP, Ladd ME, Bachert P, Radbruch A. Relaxation-compensated CEST-MRI of the human brain at 7T: Unbiased insight into NOE and amide signal changes in human glioblastoma. Neuroimage 2015;112:180-8.

26. Tang X, Dai Z, Xiao G, Yan G, Shen Z, Zhang T, Zhang G, Zhuang Z, Shen Y, Zhang Z, Hu W, Wu R. Nuclear Overhauser Enhancement-Mediated Magnetization Transfer Imaging in Glioma with Different Progression at 7 T. ACS Chem Neurosci 2017;8:60-6.

27. Goerke S, Soehngen Y, Deshmane A, Zaiss M, Breitling J, Boyd PS, Herz K, Zimmermann F, Klika KD, Schlemmer HP, Paech D, Ladd ME, Bachert P. Relaxation-compensated APT and rNOE CEST-MRI of human brain

28. Wu Y, Zhou IY, Lu D, Manderville E, Lo EH, Zheng H, Sun PZ. pH-sensitive amide proton transfer effect dominates the magnetization transfer asymmetry contrast during acute ischemia-quantification of multipool contribution to in vivo CEST MRI. Magn Reson Med 2018;79:1602-8.

29. Zhang XY, Wang F, Afzal A, Xu J, Gore JC, Gochberg DF, Zu Z. A new NOE-mediated MT signal at around -1.6ppm for detecting ischemic stroke in rat brain. Magn Reson Imaging 2016;34:1100-6.

30. Tee YK, Abidin B, Khrapitchev A, Sutherland BA, Larkin J, Ray K, Harston G, Buchan AM, Kennedy J, Sibson NR, Chappell MA. CEST and NOE signals in ischemic stroke at 9.4T evaluated using a Lorentzian multi-pool analysis: a drop, an increase or no change? Proc Int Soc Magn Reson Med 2017;25:3782.

31. Zhang XY, Wang F, Jin T, Xu J, Xie J, Gochberg DF, Gore JC, Zu Z. MR imaging of a novel NOE-mediated magnetization transfer with water in rat brain at 9.4 T. Magn Reson Med 2017;78:588-97.

32. Zu Z, Lin EC, Louie EA, Xu J, Li H, Xie J, Lankford CL, Chekmenev EY, Swanson SD, Does MD, Gore JC, Gochberg DF. Relayed nuclear Overhauser enhancement sensitivity to membrane Cho phospholipids. Magn Reson Med 2020;84:1961-76.

33. Chang YC, Liu HQ, Chang JH, Chang YY, Lin EC. Role of the cholesterol hydroxyl group in the chemical exchange saturation transfer signal at -1.6 ppm. NMR Biomed 2020;33:e4356.

34. Sutherland BA, Buchan AM. Alteplase treatment does not increase brain injury after mechanical middle cerebral artery occlusion in the rat. Journal of Cerebral Blood Flow and Metabolism 2013;33:e1-e7.

35. Meng N, Wang J, Sun J, Liu W, Wang X, Yan M, Dwivedi A, Zheng D, Wang K, Han D. Using amide proton transfer to identify cervical squamous carcinoma/adenocarcinoma and evaluate its differentiation grade. Magn Reson Imaging 2019;61:9-15.

36. Sun PZ. Demonstration of magnetization transfer and relaxation normalized pH-specific pulse-amide proton transfer imaging in an animal model of acute stroke. Magn Reson Med 2020;84:1526-33.

37. Foo LS, Larkin JR, Sutherland BA, Ray KJ, Yap WS, Hum YC, Lai KW, Manan HA, Sibson NR, Tee YK. Study of common quantification methods of amide proton transfer magnetic resonance imaging for ischemic stroke detection. Magn Reson Med 2021;85:2188-200.

38. Larkin JR, Simard MA, Khrapitchev AA, Meakin JA, Okell TW, Craig M, Ray KJ, Jezzard P, Chappell MA, Sibson NR. Quantitative blood flow measurement in rat brain with multiphase arterial spin labelling magnetic resonance imaging. J Cereb Blood Flow Metab 2019;39:1557-69.

39. Jones CK, Polders D, Hua J, Zhu H, Hoogduin HJ, Zhou J, Luijten P, van Zijl PC. In vivo three-dimensional whole-brain pulsed steady-state chemical exchange saturation transfer at 7 T. Magn Reson Med 2012;67:1579-89.

40. Zaiss M, Xu J, Goerke S, Khan IS, Singer RJ, Gore JC, Gochberg DF, Bachert P. Inverse Z-spectrum analysis for spillover-, MT-, and T1 -corrected steady-state pulsed CEST-MRI--application to pH-weighted MRI of acute stroke. NMR Biomed 2014;27:240-52.

41. Crescenzi R, Donahue PMC, Mahany H, Lants SK, Donahue MJ. CEST MRI quantification procedures for breast cancer treatment-related lymphedema therapy evaluation. Magn Reson Med 2020;83:1760-73.

42. Wu L, Jiang L, Sun PZ. Investigating the origin of pH-sensitive magnetization transfer ratio asymmetry MRI contrast during the acute stroke: Correction of T(1) change reveals the dominant amide proton transfer MRI signal. Magn Reson Med 2020;84:2702-12.

43. Liu G, Song X, Chan KW, McMahon MT. Nuts and bolts of chemical exchange saturation transfer MRI. NMR Biomed 2013;26:810-28.

44. Zu Z. Toward more reliable measurements of NOE effects in CEST spectra at around -1.6 ppm (NOE (-1.6)) in rat brain. Magn Reson Med 2019;81:208-19.

45. Liu G, Chan KW, Song X, Zhang J, Gilad AA, Bulte JW, van Zijl PC, McMahon MT. NOrmalized MAgnetization Ratio (NOMAR) filtering for creation of tissue selective contrast maps. Magn Reson Med 2013;69:516-23.

46. Jin T, Wang P, Zong X, Kim SG. Magnetic resonance imaging of the Amine-Proton EXchange (APEX) dependent contrast. Neuroimage 2012;59:1218-27.

47. Sidiropoulos N, Sohi SH, Pedersen TL, Porse BT, Winther O, Rapin N, et al. SinaPlot: An Enhanced Chart for Simple and Truthful Representation of Single Observations Over Multiple Classes. Journal of Computational and Graphical Statistics 2018;27:673-6.

48. Clark WM. Efficacy of citicoline as an acute stroke treatment. Expert Opin Pharmacother 2009;10:839-46.

49. Rao AM, Hatcher JF, Dempsey RJ. Lipid alterations in transient forebrain ischemia: possible new mechanisms of CDP-choline neuroprotection. J Neurochem 2000;75:2528-35.

50. Bazán NG Jr. Effects of ischemia and electroconvulsive shock on free fatty acid pool in the brain. Biochim Biophys Acta 1970;218:1-10.

51. Martynov MY, Gusev EI. Current knowledge on the neuroprotective and neuroregenerative properties of citicoline in acute ischemic stroke. J Exp Pharmacol 2015;7:17-28.

52. Martí-Carvajal AJ, Valli C, Martí-Amarista CE, Solà I, Martí-Fàbregas J, Bonfill Cosp X. Citicoline for treating people with acute ischemic stroke. Cochrane Database Syst Rev 2020;8:CD013066.

53. Tietze A, Blicher J, Mikkelsen IK, Østergaard L, Strother MK, Smith SA, Donahue MJ. Assessment of ischemic penumbra in patients with hyperacute stroke using amide proton transfer (APT) chemical exchange saturation transfer (CEST) MRI. NMR Biomed 2014;27:163-74.

54. Sun PZ, Zhou J, Weiyun W, Huang J, van Zijl PCM. Characterizing the evolution of the ischemic penumbra using pH weighted imaging: Journal of Cerebral Blood Flow & Metabolism 2005;25:S457.

55. Sun PZ, Zhou J, Sun W, Huang J, van Zijl PC. Detection of the ischemic penumbra using pH-weighted MRI. J Cereb Blood Flow Metab 2007;27:1129-36.

56. Kraff O, Quick HH. 7T: Physics, safety, and potential clinical applications. J Magn Reson Imaging 2017;46:1573-89.

57. Guo Y, Zhou IY, Chan ST, Wang Y, Mandeville ET, Igarashi T, Lo EH, Ji X, Sun PZ. pH-sensitive MRI demarcates graded tissue acidification during acute stroke - pH specificity enhancement with magnetization transfer and relaxation-normalized amide proton transfer (APT) MRI. Neuroimage 2016;141:242-9.

58. Zhang XY, Wang F, Li H, Xu J, Gochberg DF, Gore JC, Zu Z. Accuracy in the quantification of chemical exchange saturation transfer (CEST) and relayed nuclear Overhauser enhancement (rNOE) saturation transfer effects. NMR Biomed 2017;30:10.1002/nbm.3716.

59. Jin T, Wang P, Hitchens TK, Kim SG. Enhancing sensitivity of pH-weighted MRI with combination of amide and guanidyl CEST. Neuroimage 2017;157:341-50.

60. Foo LS, Yap WS, Hum YC, Manan HA, Tee YK. Analysis of model-based and model-free CEST effect quantification methods for different medical applications. J Magn Reson 2020;310:106648.

61. Zhang L, Liang Y, Chen Y, Li G, Zhang M, Zhao Y, et al. Enhanced CEST MRI Using the Residual of Inversed Z-Spectra for Ischemia Detection. IEEE Access 2020;8:147323-36.

62. Foo LS, Yap WS, Tee YK. Determination of

computationally efficient multi-pool model fitting approach for pulsed chemical exchange saturation transfer MRI. In: ACM International Conference Proceeding Series. Beijing: ACM; 2019. p. 32-9.

63. Tee YK, Harston GWJ, Blockley NP, Frost R, Okell TW, Thandeswaran S, Sheerin F, Jezzard P, Kennedy J, Payne S, Chappell M. Can nuclear overhauser enhancement mediated chemical exchange saturation transfer (NOE-CEST) offer a new insight in acute stroke diagnosis? Proc Int Soc Magn Reson Med 2015;23:17.

Appendix 1

Average values and CNR of AREX(3.5 ppm) and AREX(2 ppm)

AREX(2 ppm) was calculated according to Eq. [2] from the main text, with reference signal as the opposite signal at –2 ppm, i.e., Z(–2 ppm). Supplementary *Figure S1* shows the average AREX values and contrast-to-noise ratio (CNR) of the AREX(3.5 ppm) and AREX(2 ppm) of all five animals. The left column shows the average AREX values of the ischemic and non-ischemic tissues, along with the corresponding standard deviations represented by the shaded regions. APT and amine effect were decreased in ischemic tissue, in line with previous study (28). The corresponding CNR between the ischemic and non-ischemic tissues are shown in the right column. Similar to NOE(–1.6 ppm), the AREX CNR of amide and amine were maximized at 276° flip angle (FA).

Previous studies have found the optimal saturation power for maximum NOE(–1.6) effect to be 0.5 µT in human (64) and 1.0 µT in rat brain (31) at 9.4 T. Although this may maximize the NOE(–1.6) effect observed in normal tissue, it may not necessarily produce the highest CNR in the diseased tissue, as shown in the results of the present study (*Figure 3* in the main text), equivalent average saturation powers used from approximately 0.5 to 1 µT. In the case of ischemic stroke, the optimal FA for maximum NOE(–1.6 ppm) CNR was found to be 276° (equivalent to 0.82 µT continuous wave saturation). The differences in the optimal power for the same effect may be due to the different subjects scanned, acquisition parameters and quantification methods used. During clinical investigation, clinicians usually evaluate the acquired or quantified images only, thus the CNR between the normal and ischemic tissue becomes more important than merely maximizing the signal intensity of the image. Other endogenous CEST effects—amide at 3.5 ppm and amine at 2 ppm also produced maximum AREX CNR at 276° (*Figure S1*). Thus, for the saturation scheme and quantification methods used here, the optimal FA for maximum CNR between ischemic and non-ischemic tissue for the endogenous CEST effects is around 276° (~0.82 µT). This is generally in agreement with the reported optimal power for low exchange rate protons, especially for NOE(–1.6 ppm) due to its close frequency separation with the water signal; higher power will lead to larger direct saturation and diminish the NOE signal (29,44).

Magnetization transfer ratio asymmetry at 3.5 ppm [MTRasym(3.5 ppm)]

As previously recommended (37), to ease the comparisons of existing and future studies, magnetization transfer ratio asymmetry at 3.5 ppm, $MTR_{asym}(3.5\ ppm)$ was calculated from animal CEST data as:

$$MTR_{asym}(3.5\ ppm) = Z(-3.5\ ppm) - Z(3.5\ ppm) \qquad [1]$$

The relative $MTR_{asym}(3.5\ ppm)$, $rMTR_{asym}(3.5\ ppm)$ was then calculated as:

$$rMTR_{asym}(3.5\ ppm) = \frac{MTR_{asym}(3.5\ ppm)}{\left| mean\left(MTR_{asym\_normal}(3.5\ ppm) \right) \right|} \qquad [2]$$

Figure S2 shows the $MTR_{asym}(3.5\ ppm)$ images of three representative animals (Animal 1–3) at the three FAs: 184°, 276°, and 366° The composite relative $MTR_{asym}(3.5\ ppm)$ within the ADC deficit and corresponding contralateral areas all five animals are shown in the bottom row. Two-tailed paired *t*-test revealed the relative $MTR_{asym}(3.5\ ppm)$ of all animals to be significantly decreased in the ADC deficit, in line with the majority of previous publications (37).

Simulation of NOE(–1.6 ppm) in ischemic and non-ischemic tissues

A six-pool CEST model consisting of water (0 ppm), amide (3.5 ppm), magnetization transfer (0 ppm), amine (2 ppm), and NOE effects at –3.5 and –1.6 ppm was simulated using the modified Bloch equations (65) in Matlabs. Field strength of 9.4 T and a saturation scheme of 50 Gaussian saturation pulses of 20 ms pulse duration and 50% duty cycle were used, in line with the experimental parameters. Four flip angles (FAs) were simulated: 92° (equivalent to 0.273 µT average power continuous wave saturation), 184°, 276°, and 366°.

CEST parameters used for the simulation for normal and ischemic conditions are presented in *Table S1*. The parameters were extracted from literature (57-62) with slight adjustments for field strength, except for the water longitudinal and transverse relaxations T_1 and T_2, which were the averaged values obtained from the *in vivo* experiment. The ischemic exchange rate of the NOE(–1.6) pool, *x* was varied between reduction by 30–50% of the normal value. Assumptions such as negligible changes in the proton concentrations were also made as the induced stroke

was in the early time point (8).

From the simulated data, NOE(−1.6 ppm) was calculated according to equation (3) in the main text, where Z(19 ppm)/Z(3.5 ppm) was used as the reference, similar to the *in vivo* experiment. In addition, the contrast between the normal and ischemic NOE(−1.6 ppm) was evaluated using equation (4) in the main text.

When the exchange rate of NOE(−1.6) was decreased by 44% of the normal value (ischemic exchange rate =28 Hz) to simulate the ischemic tissue, it produced a decreased ischemic NOE(−1.6 ppm) (*Figure S3A*), in line with the experimental findings. While the simulated ischemic and non-ischemic NOE(−1.6 ppm) both increased with FA, similar to *in vivo*, the simulated values of both tissues were slightly lower than that of the experiment across all FAs. This could be due to the far away saturated offset (±300 ppm) treated as the unsaturated signal,

slight differences in the water relaxation values and/or magnetization transfer parameters used. Likewise, the contrast of the simulated data was found to align well with the trend of the CNR of the experimental data, increasing from 92° to 276°, peaking at 276°, before decreasing at 366° FA (*Figure S3B*).

References

64. Zaiss M, Schuppert M, Deshmane A, Herz K, Ehses P, Füllbier L, et al. Chemical exchange saturation transfer MRI contrast in the human brain at 9.4 T. Neuroimage. 2018;179:144-55.
65. Woessner DE, Zhang S, Merritt ME, Sherry AD. Numerical solution of the Bloch equations provides insights into the optimum design of PARACEST agents for MRI. Magn Reson Med 2005;53:790-9.
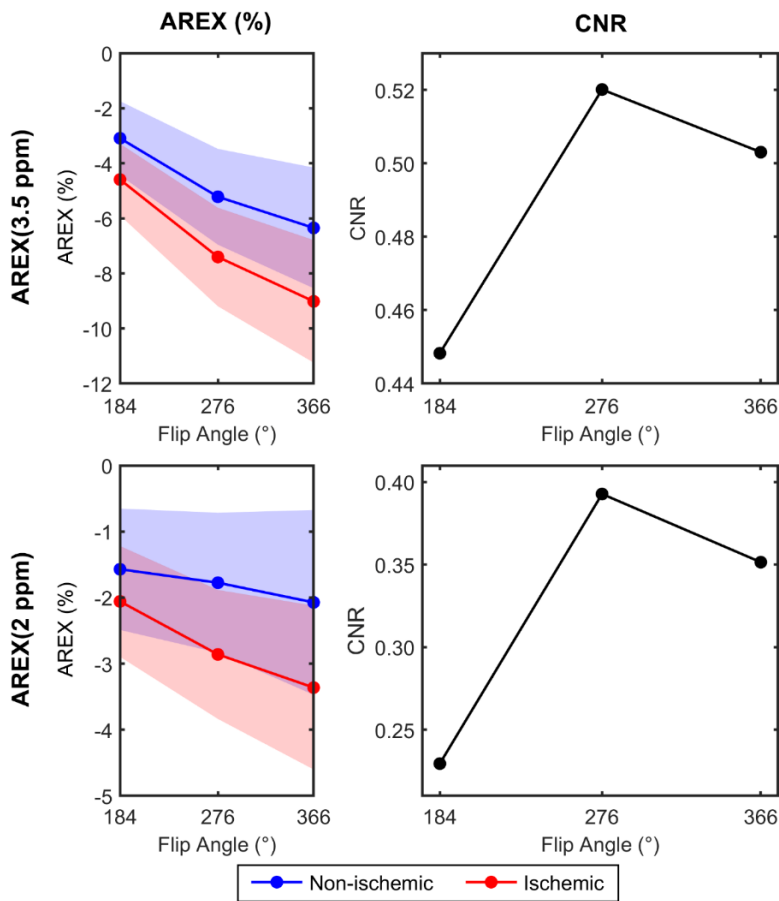
Figure S1 Average AREX values of ischemic and non-ischemic tissue, and the corresponding CNR of AREX(3.5 ppm) and AREX(2 ppm). The shaded region represents the standard deviations of the quantified AREX values. AREX, apparent exchange-dependent relaxation; CNR, contrast-to-noise ratio.
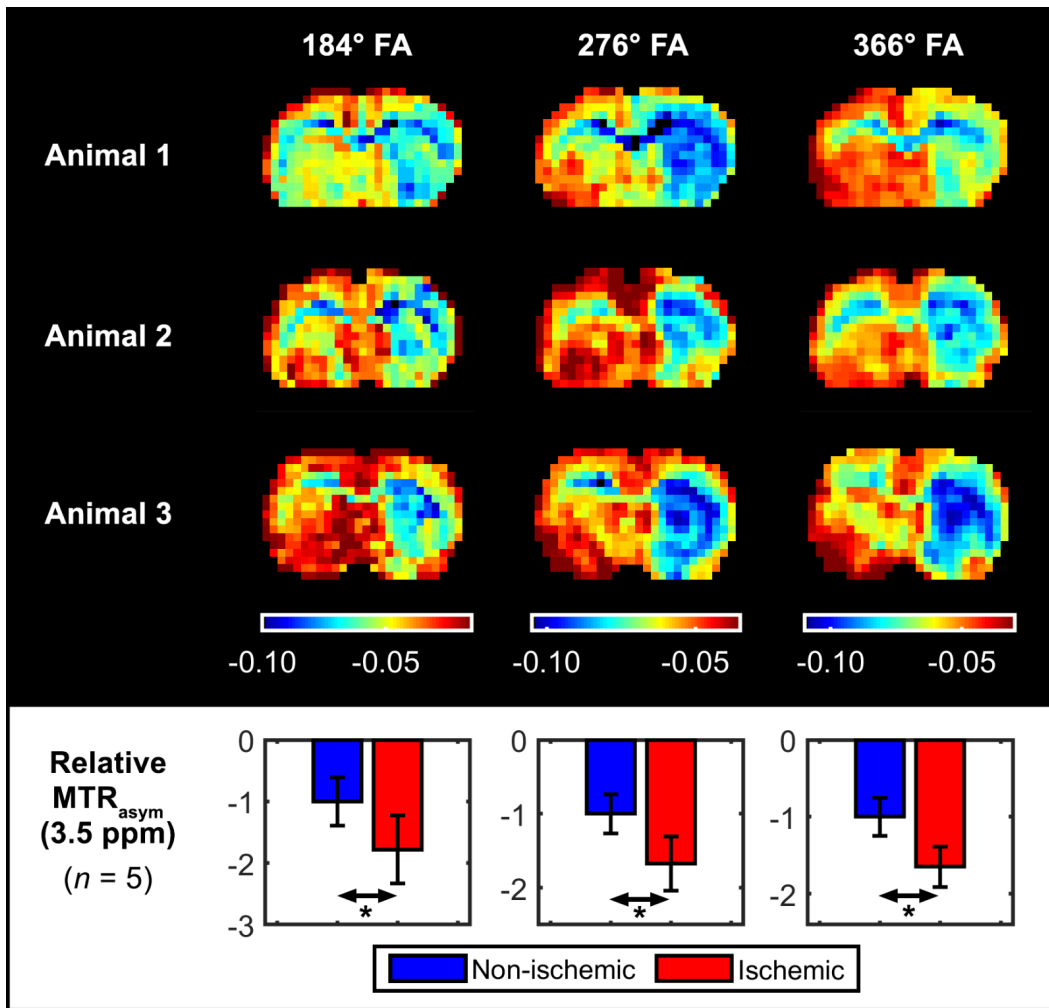
Figure S2 A The MTRasym(3.5 ppm) maps of three representative animals (Animals 1–3) and the composite relative MTRasym(3.5 ppm) of all five animals at three saturation flip angles: 184º, 276º, and 366º. *, $P<0.05$. MTRasym, magnetization transfer ratio asymmetry; FA, flip angle.
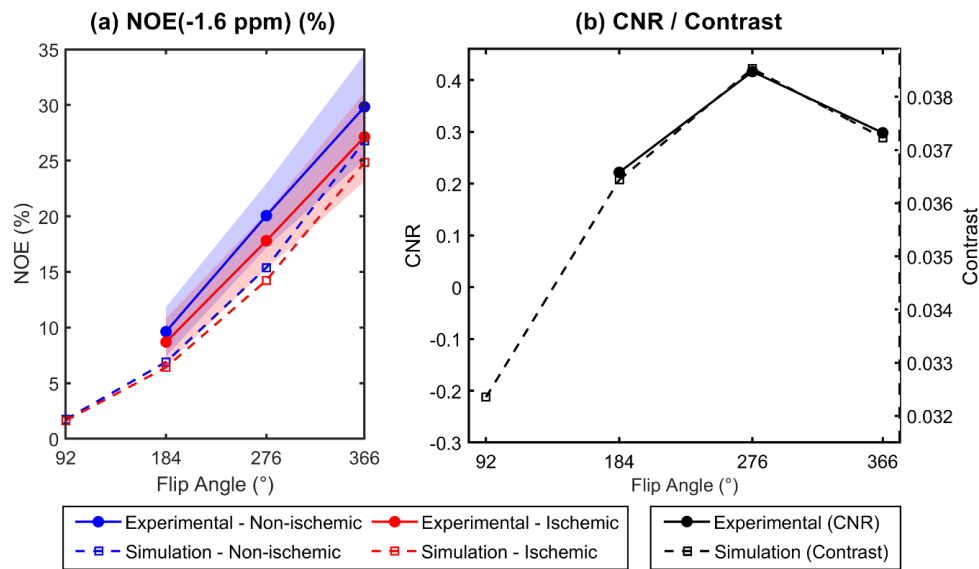
Figure S3 NOE(–1.6 ppm) and CNR/contrast of the simulated and experimental data. (A) Simulated NOE(–1.6 ppm) and average experimental NOE(–1.6 ppm) of ischemic and non-ischemic tissues; the shaded areas represents the standard deviations of the experimental NOE(–1.6 ppm). (B) CNR or contrast between the two tissues of experimental and simulated data respectively. NOE, nuclear Overhauser enhancement; CNR, contrast-to-noise ratio.

Table S1 Six-pool CEST data simulation parameters taken from literature (57-61)

CEST Pools	Water	Amide	MT	NOE	Amine	NOE
Chemical shift (ppm)	0	3.5	0	–3.5	2	–1.6
T1 (s)						
Normal	1.63	1.63	1.63	1.63	1.63	1.63
Ischemic	1.83	1.63	1.63	1.64	1.63	1.63
T2 (ms)						
Normal	40.16	20.00	0.02	0.40	38	0.4
Ischemic	38.68	20.00	0.02	0.40	38	0.4
Exchange rate (Hz)						
Normal	–	30	25	50	1,000	50
Ischemic	–	18	25	50	500	x*
Concentration (M_{0a})						
Normal	1	0.001	0.1	0.007	0.002	0.003
Ischemic	1	0.001	0.1	0.007	0.002	0.003

*, varied between 30–50% reduction from 50 Hz. CEST, chemical exchange saturation transfer; NOE, nuclear Overhauser enhancement; MT, magnetization transfer.